Powder Technology 212 (2011) 410–417

Contents lists available at ScienceDirect

Powder Technology

journal homepage: www.elsevier.com/locate/powtec

Preparation, characterization and photoactivity of TiO_2 obtained by a reverse microemulsion route

C.E. Zubieta [a,d,*], J.F.A. Soltero - Martínez [b], C.V. Luengo [c,d], P.C. Schulz [a]

[a] Departamento de Química e INQUISUR (CONICET), Universidad Nacional del Sur, Bahía Blanca, Argentina
[b] Departamento de Ingeniería Química, CUCEI, Universidad de Guadalajara, Guadalajara, Mexico
[c] Departamento de Física, Universidad Nacional del Sur, Bahía Blanca, Argentina
[d] CONICET, Argentina

ARTICLE INFO

Article history:
Received 22 December 2010
Received in revised form 14 May 2011
Accepted 17 June 2011
Available online 2 July 2011

Keywords:
Titania
Microemulsion
Photodegradation
Pollution
Methylene blue
Adsorption

ABSTRACT

TiO_2 was synthesized by a reverse microemulsion route. By using different water contents in the reverse microemulsion, we obtained three different materials named R = 10, R = 20 and R = 30. The reverse microemulsion synthesis has the advantage that the kind of the crystalline titania structure obtained may be changed by simply modifying the water content in the microemulsion.
The synthesized materials were characterized by nitrogen adsorption, scanning and transmission electron microscopy, and X-ray diffraction. Methylene blue (MB) was used as testing dye; we studied the pH effect and catalyst dosage in the MB photodegradation. The degradation kinetics was also studied.

1. Introduction

Textile industries require the use of vast amounts of water and chemicals, and their effluents have important effects on environmental quality. Being highly water-soluble, it is estimated that 10–20% of dyes remains in the wastewater during the production process of such dyes [1] and nearly 50% of dyes may be lost to the effluent during dying process of cellulose fibers [2]. Therefore, about 400 tonnes daily [3] finds their way into the environment, primarily dissolved or suspended in water.

Adsorption is a physicochemical wastewater treatment process, which is gaining prominence as a means of producing high quality effluents, which are low in concentrations of dissolved organics.

Semiconductor photocatalysis has attracted a great deal of attention in recent years. The strong oxidative power of photogenerated holes on semiconductor surface has made them a most suitable photocatalytic material in environmental remediation. Photoexcitation of semiconductors generates electron–hole pairs capable of attracting organic dyes either directly or indirectly by means of highly reactive species during their reaction with the solvent and/or additives [4–6].

In general TiO_2 is recognized as the most efficient, nontoxic, and stable photocatalyst. Mechanistically, the photocatalyst TiO_2 is first excited by UV light and subsequently initiates the photodegradation process. Their unique properties [7] have found applications in areas, such as pigments [8], cosmetics [9], catalysts [10], photocatalyst [11], etc. During the past two decades, many synthetic methods have been proposed to obtain mesoporous titanium dioxide, including sol–gel method, template method, hydrothermal method, solvothermal method, ultrasound-induced method, ion liquid method, and evaporation-induced self-assembly method [12]. Mesoporous TiO_2 using synthesized by conventional approaches using surfactants as templates has poor photocatalytic activity because the surfactant is bound very tightly to the mesoporous TiO_2 as a result of which the surfactants could not be removed entirely, by either calcination below the crystallization temperature of anatase or solvent extraction [13].

The aim of this work is to evaluate the elimination (by adsorption plus photodegradation) of methylene blue dye by the utilization of three TiO_2 nanoparticles obtained from an Aerosol OT (AOT, $C_{20}H_{37}NaO_7S$)/hexane/water reverse microemulsion. The synthesis of nanoparticles via inverse microemulsions was used previously by many authors. The preparation method using extremely small water pools in reverse micelles as the reaction media has been studied extensively. One of the advantages of this method is that localized supersaturation of the reactants is suppressed and a uniform nucleation occurs, since the reactants are dispersed very well in the reverse micellar solution. In addition, the reverse micelles can protect the nanoparticles against excessive aggregation. As examples, CdS nanoparticles have been prepared in reverse micellar solutions such

* Corresponding author. Tel.: +54 291 154710377, +54 291 4595100int3523.
E-mail address: czubieta@uns.edu.ar (C.E. Zubieta).

0032-5910/$ – see front matter © 2011 Elsevier B.V. All rights reserved.
doi:10.1016/j.powtec.2011.06.017

as AOT/isooctane or AOT/heptane systems [14–18]. We also investigated the effect of concentration of water as well as R ratio on the TiO_2 particles as a photocatalyst for the decomposition of MB.

We analysed how different water contents in reverse microemulsion affected the MB degradation. Also we attempt to evaluate the pH effect and TiO_2 dosage in the performance of TiO_2 focused on environmental applications.

Methylene blue (MB) is a cationic dye, extensively used for cotton dying and papers, wool and silk colouring. The effects of the presence of dyes in wastewater could be eye burning effect, nausea, vomiting and diarrhoea [19]. The synthesized materials were characterized by X-ray powder diffraction (XRD), Scanning Electron Microscopy (SEM), Transmission Electron Microscopy (TEM) and Nitrogen adsorption isotherms.

2. Experimental

2.1. Preparation of catalysts

Sodium dioctyl sulfosuccinate (Aerosol OT; AOT) 99% was obtained from Sigma. A reverse microemulsion solution was prepared by dissolving 1.1276 g AOT in 0.46 g of water. Then the mixture above mentioned was left 3 h for the surfactant hydration to be produced. In this case the water/AOT molar ratio (R) was R = 10. Then 80 mL of n-hexane (Carlo Erba, p.a.) were added and the system was sonicated to produce the microemulsion. Then 1.4 mL of $TiCl_4$ (Carlo Erba, 99%, $\delta = 1.722\ g/cm^3$) was added and left three days to react following the reaction:

$$2H_2O_{(l)} + TiCl_{4\ (l)} \rightarrow TiO_{2\ (s)} + 4HCl_{(g)} \quad (1)$$

The excess of HCl and n-hexane was eliminated by evaporation under vacuum. The resulting material was left 3 h in hydrothermal treatment at 70 °C in autoclave to force hydrolytic precipitation [20]. A white powder composed by the titania nanoparticles surrounded by AOT was obtained, and was then calcinated during 7 h at 540 °C under air flux for a complete crystallization and surfactant elimination. In two other syntheses, R were altered into 10, 20 and 30 (modifying the water content to the values 0.5, 1.0 and 1.5 g), and so, three different TiO_2 materials (called R = 10, R = 20 and R = 30 respectively) were obtained.

Methylene blue (MB) was chosen as adsorbate. MB is a basic blue dyestuff ($\lambda_{max} = 664$ nm, $M_w = 373.9\ g\ mol^{-1}$). Aqueous dye solutions were prepared by using only double distilled water. For the degradation test we studied the remotion of MB in different buffered solutions; citrate/citric acid (pH = 4.0), monobasic sodium phosphate/dibasic sodium phosphate (pH = 8.0) and carbonate/carbonic acid (pH = 10.0).

2.2. Characterization

2.2.1. X-ray diffraction analysis

Powder X-ray diffraction (XRD) experiments were performed in a Philips PW 1710 diffractometer with CuK_α radiation ($\lambda = 1.5418$ Å) and graphite monochromator operated at 45 kV; 30 mA and 25 °C.

2.2.2. Nitrogen adsorption isotherms

The nitrogen adsorption isotherms were measured at 77.6 K with a Micrometrics Model Accelerated Surface Area and Porosimetry System (ASAP) 2020 instrument. Each sample was degassed at 373 K for 720 min at a pressure of 10^{-4} Pa.

2.2.3. Transmission electron microscopy (TEM)

Transmission electron microscopy was performed using a JEOL 100 CX transmission electron microscope, operated at 100 kV with magnification of 100,000×. Observations were made in a bright field. Powdered samples were placed on cooper supports of 2000 mesh.

2.2.4. Scanning electron microscopy

Scanning electron microscopy was performed using a JEOL 35 CF. Tokio, Japan.

2.3. Adsorption test

Adsorption experiments (in darkness to avoid photodegradation) were carried out in 5 mL glass-stopped round bottom flasks immersed in a thermostatic shaker bath. For this, 50 mg of adsorbent were mixed with 5 mL of aqueous dye solutions with (0.0043–0.036) mmol/L concentration range. The flasks with their content were shaken at 25 °C, 35 °C and 45 °C. The stirring speed was kept constant at 90 rpm. At the end of the adsorption period, the supernatant was centrifuged for 3 min at a speed of 3500 min^{-1}. The supernatant MB concentration before and after adsorption was determined using a Spectronic −20 UV–vis spectrophotometer at 664 nm.

2.4. Photodegradation

To study the effect of the photodegradation, the same experiments were carried out in presence of UV light at T = 25 °C. A DESAGA UV 131000 lamp ($\lambda = 366$ nm) was applied as a radiation source for the photodegradation of dyes. Light intensity was estimated as $I_a = 2.7 \times 10^{-6}$ mol photon s^{-1} from the supplier's data. To discriminate between both effects (adsorption and photodegradation) the results of the experiments without light were subtracted from those carried out under irradiation.

At different irradiation times, 2 mL of the supernatant was separated and centrifuged. The change in the dye concentration before and after degradation was spectrophotometrically determined at 664 nm.

3. Results and discussion

3.1. X-ray diffraction analysis

The XRD patterns of TiO_2 powders synthesized at different [water]/[surfactant] ratio are displayed in Fig. 1. For a better view of the mentioned figure, we added 2000 and 5000 units of intensities in R = 20 and R = 30, respectively. The R = 10 material is mainly composed of anatase (2θ = 25.2°) and rutile (2θ = 27°, 35.9°). The broad peak around 40° is attributed to a mixture of anatase and rutile phases. In the R = 20 titania there is a small peak of anatase (2θ = 25.2°) but rutile peaks are increased (2θ = 27°, 35.9°).

In R = 30 material there are peaks in (2θ = 27°, 35.9°), indicating that the sample is composed of pure rutile.

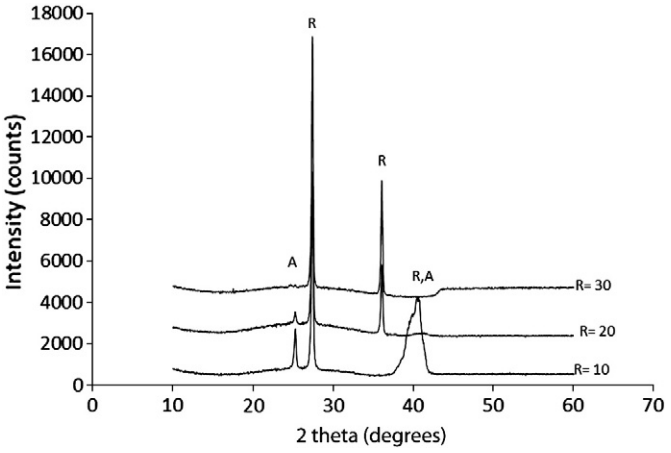

Fig. 1. X-ray diffraction patterns of TiO_2 powders prepared with different water/surfactant ratios (R). Peaks correspond to: A: anatase; R: rutile.

The composition of the different synthesized titanias was determined by using the XRD patterns and the correlations giving by Zhang and Banfield [21]. The weight fraction of rutile (WR), anatase (WA) and brookite (WB) in the sample was determined with the relationships:

$$W_A = \frac{k_A A_A}{k_A A_A + A_R + A_B A_B} \quad (2)$$

$$W_R = \frac{A_R}{k_A A_A + A_R + A_B A_B} \quad (3)$$

$$W_B = \frac{k_B A_B}{k_A A_A + A_R + A_B A_B} \quad (4)$$

where A_A, A_B and A_R are the integrated intensity of the anatase (121, $2\theta = 25.44°$), brookite (101, $2\theta = 30.98°$) and rutile (111, $2\theta = 27.54°$) respectively, obtained from the XRD patterns by deconvolution using the PeakFit program. The coefficients $k_A = 0.886$ and $k_B = 2.721$ were obtained from Ref. [21].

The composition of the different samples were R = 10 (WA = 0.071, WB = 0, WR = 0.929), R = 20 (WA = 0.036, WB = 0, WR = 0.964), R = 30 (WA = 0, WB = 0, WR = 1).

In both cases, R = 10 and R = 20 the crystalline composition of rutile is major than 92%. However, in R = 30 the only phase present is rutile.

It can be inferred that the variation in water content in the reverse microemulsion plays an important role in the kind of the crystalline phases of the titania obtained. With an increment in the water content in reverse microemulsion, the anatase crystalline phase decreases and the rutile phase increases, finally giving rise to pure rutile and an increased crystallinity, as indicated by narrower peaks. Comparison between the XRD patterns reveals that a higher crystallinity was obtained when R was 30.

3.2. Nitrogen adsorption analysis

Both specific surface areas and pore sizes of the samples were determined from the nitrogen adsorption data using Brunauer–Emmet–Teller technique [22]. The nitrogen adsorption–desorption isotherms for TiO_2 (R = 20) are shown in Fig. 2. TiO_2 R = 20 material show the typical N_2 adsorption isotherm type IV (The plot for R = 10 and R = 30 not shown here since both materials showed the same type of isotherm) [23]. It is characteristic of mesoporous materials based on IUPAC classification. The *t*-plots in Fig. 3 show the appearance of the materials having slit-shaped pores. The BET surface area, the adsorption average pore diameter by BET (4 V/A) and the single point adsorption total pore volume of pores was summarized in Table 1.

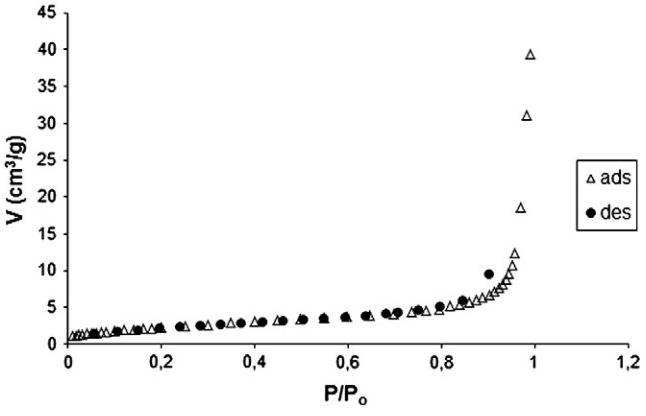

Fig. 2. Nitrogen adsorption–desorption isotherms for TiO_2 R = 20 sample. Ads (adsorption), des (desorption).

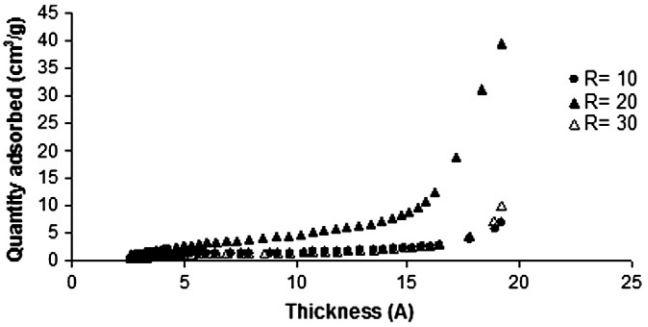

Fig. 3. *t*-plot of TiO_2 samples.

The pore sizes distribution plots of TiO_2 materials were also made (not shown). They all showed mesoporous size, based on the IUPAC classification (between 1–25 nm).

3.3. TEM micrographs

The TEM microphotographs (Fig. 4) of all materials are in agreement with the existence of a lamellar structure with slit-shaped pores. For R = 10 particles have a nearly isometric shape with some platelet-shaped crystals. Particles seem to be formed by small, compact crystals. When R increases additional water is included in the "pool" and the inverse micelle swells giving larger titania particles (R = 20) which seem to be partially agglomerated showing an increased porosity when compared with R = 10. A further increment in water content causes a porous agglomeration of particles. It is difficult to control the agglomeration of the particles using the microemulsion method but it is possible to control at the relatively low concentration of water, as it can be seen in R = 10 and R = 20 titania. We found a similar behavior in the preparation of nanosized TiO_2 via hydrolysis of titanium tetraisopropoxide in AOT reverse micelles [24].

3.4. SEM micrographs

The SEM microphotographs (Fig. 5A–D) show that the increase of R from 10 (Fig. 5A) to 30 (Fig. 5C–D) causes the microemulsion conversion from inverse micelles (R = 10 and R = 20 (Fig. 5B)) to a bicontinuous system (R = 30). This is in agreement with the particle size. Such structure can be a deformation of lamellar mesophase.

3.5. Adsorption kinetics test

Traditionally, adsorption kinetics is described following the expressions originally given by Lagergren, which are special cases for the general Langmuir rate equation [25]. A simple kinetic analysis of adsorption is the pseudo-first order equation in the form:

$$\frac{dq_t}{d_t} = k_{1,s}(q_e - q_t) \quad (5)$$

Table 1
Nitrogen adsorption data of the TiO_2 samples prepared by inverse microemulsion. A_{BET}: BET surface area, D_{aap}: adsorption average pore diameter by BET (4 V/A), V_{spat}: single point adsorption total pore volume of pores.

Sample TiO_2	A_{BET} (m^2/g)	D_{aap} (Å)	V_{spat} (cm^3/g)
R = 10	3.88	92.57	0.008
R = 20	8.21	234.91	0.048
R = 30	3.82	116.80	0.011

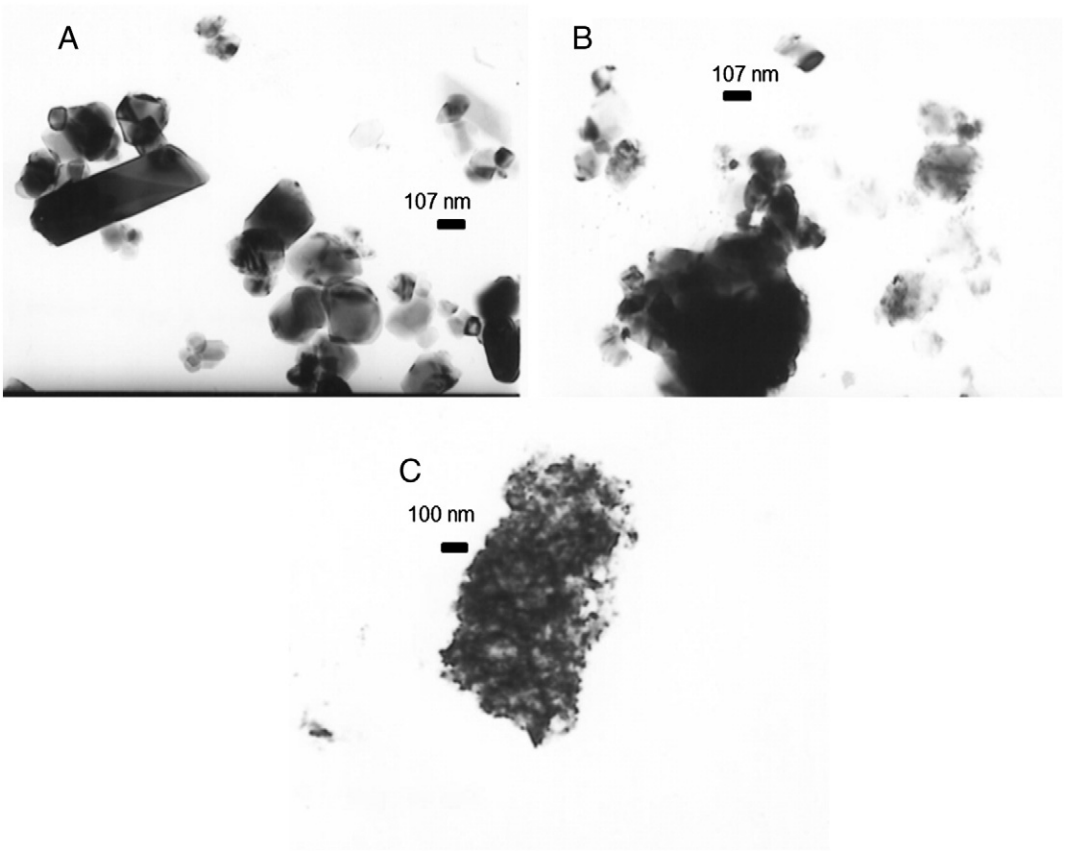

Fig. 4. TEM micrographs for TiO_2 (A) R = 10; (B) R = 20; (C) R = 30. The bar represents 107 nm (R = 10 and R = 20), and 100 nm (R = 30).

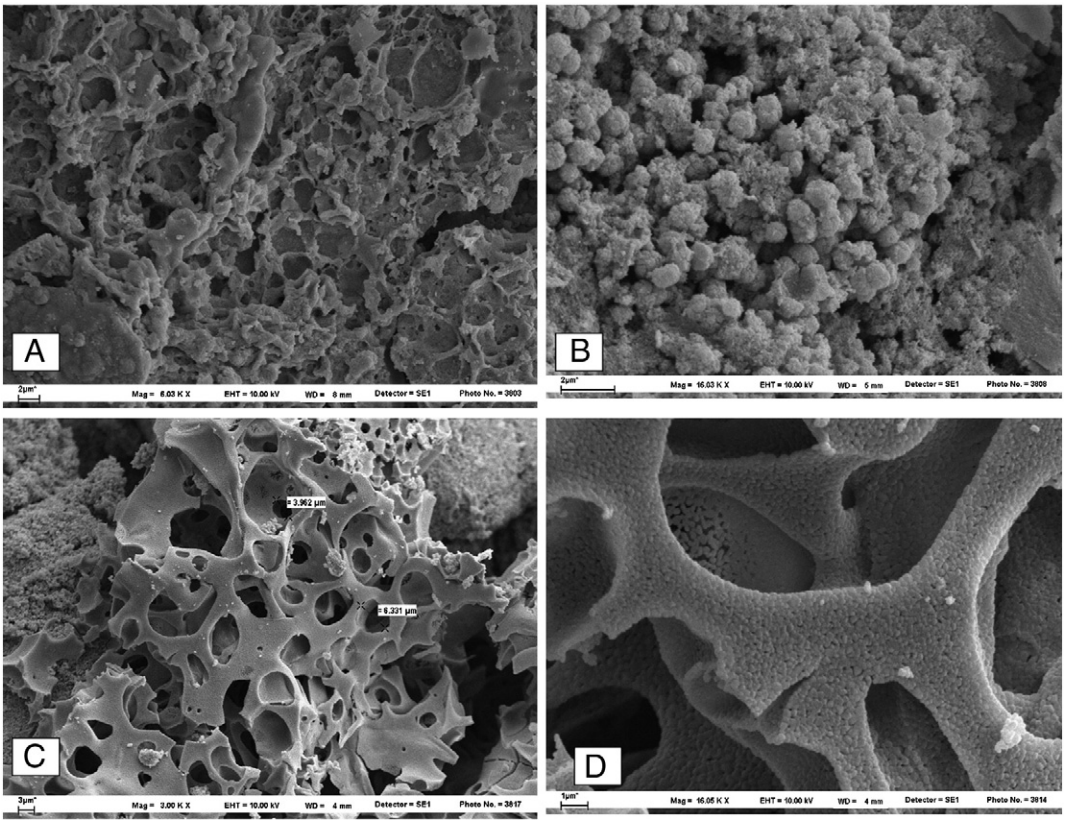

Fig. 5. SEM micrographs for TiO_2 (A) R = 10; (B) R = 20; (C) R = 30.

where $k_{1,s}$ is the pseudo-first order rate constant and q_e denotes de amount of adsorption at equilibrium. Integrating Eq. (5) for the boundary conditions t = 0 to t and $q_t = 0$ to q_t gives:

$$\ln(q_e - q_t) = \ln(q_e) - k_{1,s}t \tag{6}$$

In addition, a pseudo-second order equation based on adsorption equilibrium capacity may be expressed in the form:

$$\frac{dq_t}{dt} = k_{2,s}(q_e - q_t)^2 \tag{7}$$

where $k_{2,s}$ is the pseudo-second order rate constant. By integrating and applying the initial conditions and rearranging to obtain a linear form, we have:

$$\frac{t}{q_t} = \frac{1}{k_{2,s}q_e^2} + \frac{1}{q_e}t \tag{8}$$

The fitting validity of these models is traditionally checked by the linear plots of ln $(q_e - q_t)$ vs. t and t/q_t vs. t, respectively. The slope and intercept of the obtained straight line provide the kinetic constant and the q_e parameters, respectively.

3.5.1. Intra-particle diffusion control

The adsorption mechanism of adsorbate onto adsorbent follows three steps: film diffusion, pore diffusion and intra-particle transport. In order to investigate the possibility of intra-particle diffusion resistance affecting the adsorption, the intra-particle diffusion model [26] was explored:

$$q_t = kt^{1/2} + I \tag{9}$$

where k is the intra-particle diffusion rate constant. Fig. 6 shows the kinetic results. Two different steps may be seen, one of them at t<200 h and the other at times between 200 and 1000 h. The experimental data are satisfactorily fit the pseudo-second order model at all studied temperatures for short times. Kinetic parameters have been summarized in Table 2. However, at long times experimental data fit to Eq. (9). A linear dependence of q_t on $t^{1/2}$ was found at all temperatures that suggest that the internal diffusion mechanism is significant in the MB adsorption. Since the lines in Fig. 6 do not pass through the origin, it follows that the diffusion mechanism is not the only one involved in the MB adsorption kinetics. The intra-particle diffusion predominates at shorter times when the adsorbent is changed from R = 10 to R = 30. This situation may be related to the increasing porosity that may be seen in the TEM and SEM images

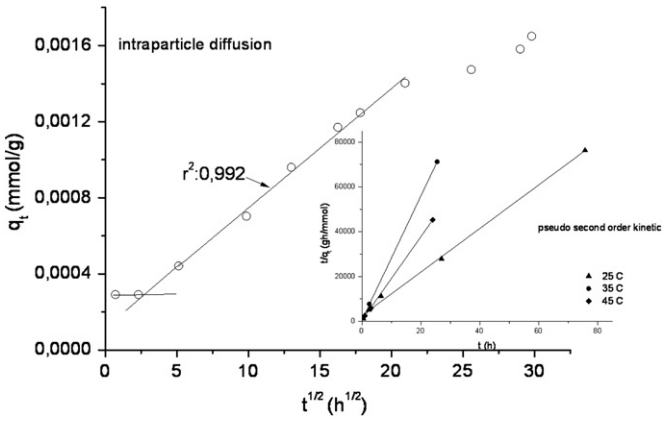

Fig. 6. Intra-particle diffusion plot for MB adsorption onto TiO_2 R = 30 for long times. Inset: Pseudo-second order kinetics for MB onto TiO_2 R = 20 for the initial period of adsorption.

Table 2
Pseudo-second order kinetics parameters for the adsorption of MB on TiO_2 samples.

	$q_{e,2}$ (mmol/g) × 1 × 10^{-4}	k_2 (g/mmol h)	r^2
TiO_2 R = 10			
25 °C	7.88	401.12	0.982
35 °C	5.19	579.91	0.998
45 °C	8.19	199.7	0.981
TiO_2 R = 20			
25 °C	10.26	373.08	0.996
35 °C	3.60	14925	0.999
45 °C	5.35	7862	0.999
TiO_2 R = 30			
25 °C	2.91	11526	0.994
35 °C	4.63	1364	0.977
45 °C	–	–	–

when passing from R = 10 to R = 30. Then, the external adsorption site may reduce their influence *vis-à-vis* the internal ones, and the intra-particle diffusion is increasingly the dominant mechanism determining the MB adsorption velocity.

3.6. Photocatalytic activity

3.6.1. pH effect

Samples were made with 0.2 g of catalyst in 10 mL of dye solution. The photodegradation of MB (expressed in %) as a function of pH for all powders is shown in Fig. 7. It should be noted that the photocatalytic degradation of MB was dependent on the synthesis conditions of the TiO_2 particles [27].

A blank study was made to check MB degradation without TiO_2 material. In these conditions no MB degradation was detected at pH = 4 and pH = 10, while at pH = 8 there was 4% of dye degradation.

We noticed that the maximum MB remotion in pH = 4 was 45% in 8 h for R = 20 material. The performance of R = 10 was lower than that in R = 20, reaching a 37% of degradation of MB in the same period of time. R = 30 does not show any degradation of MB in acid conditions.

At both higher pH values (pH = 8.0 and pH = 10.0) the MB remotion was better than that in acid conditions, and the highest remotion was attained at pH = 10 for the lowest R content material. R = 30 material shows the worst activity. MB degradation reached 98% of remotion in 7.5 h for R = 10 titania in pH = 10.

The different TiO_2 performance observed in Fig. 7 could explain as follows. In an aqueous system, TiO_2 is amphoteric [28]. The TiO_2 surface is predominantly negatively charged when the pH is higher than the TiO_2 isoelectric point. As the pH decreases, the functional groups are protonated, and the proportion of the positively charged surface increases. Thus, the surface of titania would be negatively charged and adsorb cationic MB easily under pH > pH_{zpc} (zero point charge) conditions. Under acidic conditions, it was difficult for cationic MB dye to adsorb onto TiO_2 surface. With the active OH radicals usually in low concentrations, the photodegradation of MB remained very slow. With higher pH values, the formation of active OH species is favored, due not only to improved transfer of holes to the adsorbed hydroxyls, but also to electrostatic attractive effects between the negatively charged TiO_2 particles and the operating MB dye. Similar results have been found in the photodegradation of malachite green on TiO_2 particles [29].

The effect of pH in the kinetics degradation of MB was studied, too. In the case of pH = 8 and pH = 10 we plotted t/q_t vs. t for all materials (not shown here). It was concluded that the pseudo-second order model fits the experimental data in the entire degradation process, and confirms that the kinetics degradation of MB onto all TiO_2 materials follows a pseudo-second order kinetics model. The kinetics parameters obtained are exposed in Table 3.

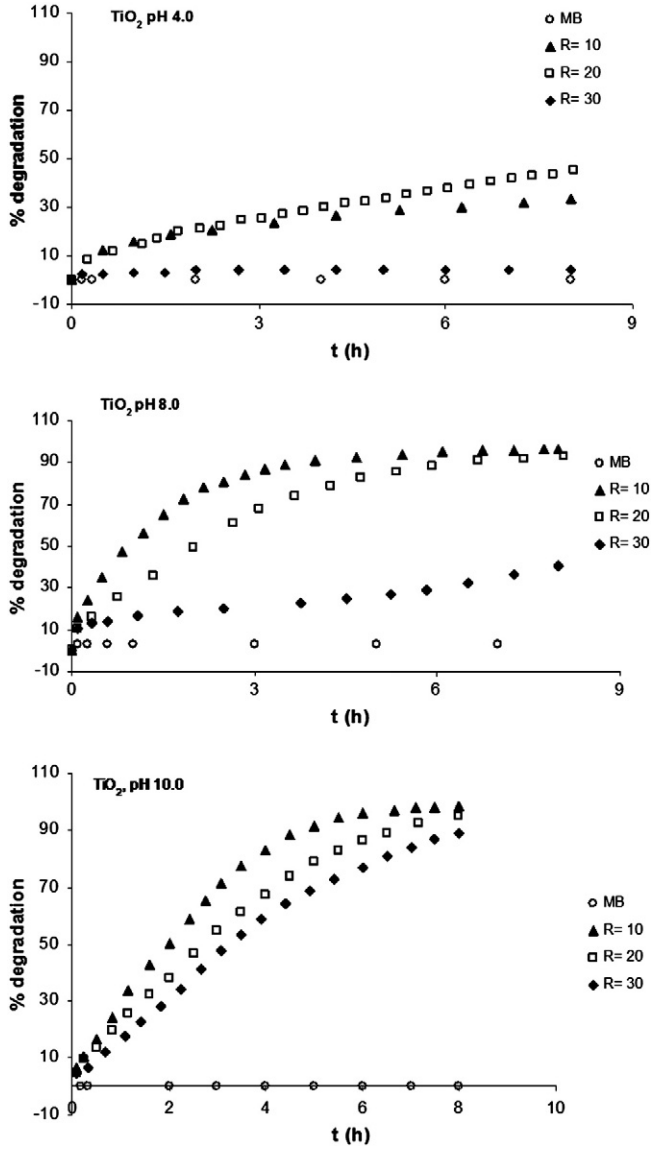

Fig. 7. Photodegradation of MB (%) on TiO_2 as a function of pH (A): pH = 10.00; (B): pH = 8.00; (C): pH = 4.00.

In general, the kinetic degradation of MB in pH = 10 is slower than in pH = 8.0. This could be possible because the buffered solution in pH = 10.0 is composed of carbonate and bicarbonate. Both bicarbonate and carbonate are efficient scavengers of hydroxyl radicals due to their very high rate constants with the hydroxyl radicals ($k = 3.9 \times 10^8 M^{-1} 1\ s^{-1}$ for carbonate and $k = 8.5 \times 10^6 M^{-1}\ s^{-1}$ for bicarbonate) [30].

The rate constant of MB degradation is higher in R = 10 and lower in R = 30. This could be due to the fact that both R = 10 and R = 20 materials are composed of a mixture of anatase and rutile. It was found in the literature that the smaller band gap of rutile "catches" the photons, generating electron/hole pairs. The electron transfer, from the rutile conduction band to electron traps in anatase phase, takes place. Recombination is thus inhibited, allowing the hole to move to the surface of the particle and react [31]. Other authors consider that the presence of anatase/rutile combinations can be most beneficial for suppressing the recombination of photogenerated species and thus to enhance the photoactivity [32].

Table 1 shows that the surface area of R = 20 TiO_2 particles is higher than that in R = 10 and R = 20, but its photoactivity does not show the better MB remotion capacity, as we expected. This suggests that the surface area of particles and the particle size show no relationship with the photocatalytic decomposition of MB in alkaline pH values, and this result is consistent with other results [24,33]. As such, the crystalline phases presents in TiO_2 materials was more important than the surface area or the particle size of the titania particles, which is also consistent with others results found in literature [34,35].

In acid conditions, the experimental data does not fit with high correlation coefficients the pseudo-second order model. For TiO_2 R = 10, R = 20 and R = 30 the kinetics data fit very well with an intra-particle diffusion model, as demonstrated in Fig. 8. The kinetics parameters obtained are exposed in Table 3. We noticed that the higher rate degradation of MB was found in R = 20 titania. As we have been able to infer, the kinetic degradation of experimental data fits well with intra particle model. For this reason the higher degradation rate in R = 20 could be due to the average pore diameter for R = 20 is higher than that in R = 10 and R = 30.

3.6.2. Effect of photocatalytic dosage

Fig. 9 shows the degradation of MB (expressed in %) on TiO_2 R = 10, employing different quantities of catalyst from 0.1 g to 0.4 g. The pH was fixed in 10.0 in all cases.

As could be expected, the MB degradation in systems with 0.1 to 0.3 g titania increased as the TiO_2 content augmented. But with 0.4 g the degradation efficiency is not increased as it was expected. In fact the degradation for 0.4 g is not significantly lower than that of 0.3 g. Its degradation curve is close to that of 0.3 g, obviously higher than that of 0.2 g. In the range of experimental error, we consider that degradation of MB is the same in both 0.3 and 0.4 g.

The effect of TiO_2 dose in the kinetics degradation of MB was studied. Fig. 10 showed a plot of t/q_t vs. t for the highest content of TiO_2 (0.4 g). It is concluded that the pseudo-second order model fits the experimental data very well in the entire degradation process, and confirms that the degradation of MB onto R = 10 in pH = 10 follows the pseudo-second order kinetics model. Similar results were obtained for MB degradation onto R = 10, in other TiO_2 contents.

Table 3
Intra particle diffusion and pseudo-second order rate constant of MB degradation onto different TiO_2 samples at different pH values.

Kinetic model	Intra-particle diffusion rate constant	Pseudo-second order rate constant	
	$k_{deg} \times 10^3$	k_{deg} (g/mmol h)	
Samples	pH 4.0	pH 8.0	pH 10.0
R = 10	0.35 ($r^2 = 0.99$)	491.9 ($r^2 = 0.99$)	176.4 ($r^2 = 0.98$)
R = 20	0.48 ($r^2 = 0.99$)	118.16 ($r^2 = 0.99$)	73.77 ($r^2 = 0.97$)
R = 30	–	–	41.49 ($r^2 = 0.98$)

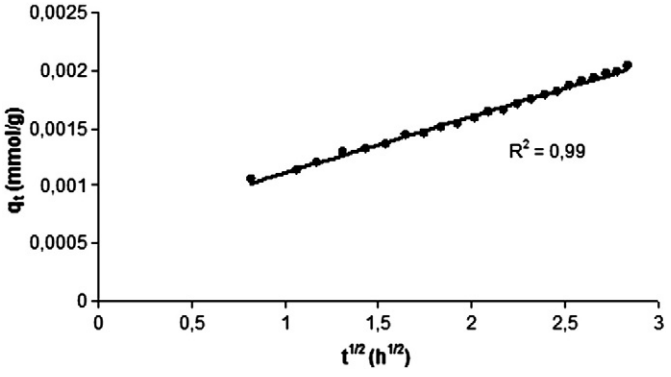

Fig. 8. Intra-particle diffusion model for TiO_2 R = 20 in pH = 4.0.

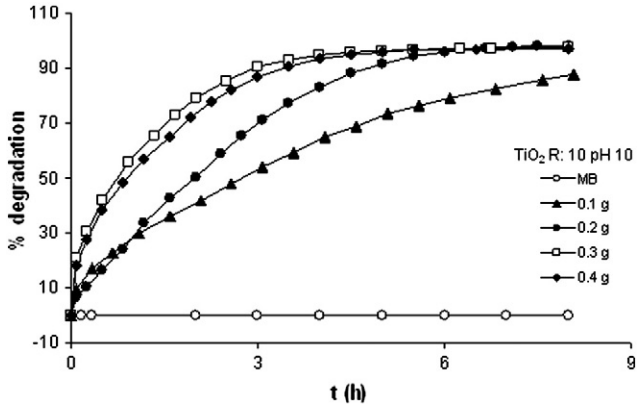

Fig. 9. Effect of photocatalytic dosage for TiO_2 R = 10 in pH = 10.0.

These plots are not shown here. The obtained results are exposed in Table 4. From this table, it is obvious that k_{deg} values are similar when the catalyst contents are 0.1 and 0.2 g. This means that there is no difference in the degradation rate for the decomposition of MB with 0.1 and 0.2 g of TiO_2. However, it is interesting to note that the degradation rate increases with the increase in catalyst content from 0.2 to 0.3 reaching a maximum, and then decreases again with a new increment in titania content from 0.3 to 0.4 g. This fact may be caused by aggregation of TiO_2 particles at high concentrations (0.4 g) causing a reduction in the interfacial area between the reaction solution and the photocatalyst. Thus, the number of surface active sites on the catalyst surface is decreased [36] and an augment in degradation rate of MB is not observed with 0.4 g of titania. Other reason could be that at very high TiO_2 content, the intensity of UV radiation in the suspension was attenuated because of turbidity and increased light scattering [37]. As a consequence, this study shows the necessity of choosing the exact amount of TiO_2 added to the sample to ensure the maximum efficiency in the degradation of MB, which is especially important in the elimination of dyes from textile effluents.

4. Conclusions

TiO_2 particles were synthesized in AOT reverse microemulsion. The crystalline composition, the size of particles and their porosity were affected by the water content in the reverse micelles.

The experimental data of methylene blue (MB, used as a probe) adsorption initially follows a pseudo-second order kinetics, while after a long time the plots of q_t vs. $t^{1/2}$ exhibited two linear sections with different slopes, indicating that two different intra-particle diffusion steps occurred in the dye adsorption process.

Under the same reaction condition, the intrinsic characteristics of photocatalysts have a complex effect on the ultimate photocatalytic activity [38]. According to our research, the best photocatalytic MB decomposition was at pH = 10.0 and the tested material showing the best MB photodegradation activity was composed by a mix of anatase and rutile instead of that of pure rutile. The photocatalytics degradation on the decomposition of MB has no relationship with the specific area and particle size but it increases with a high content in anatase phase. An increase of the titania content in the sample first increases the photodegradation, which passes through a maximum and then no obvious augment is shown when TiO_2 is added, because of an increased turbidity.

From this study we concluded that the TiO_2 R = 10 is the best material to remove MB in an alkaline medium using ultraviolet light as source of radiation. TiO_2 R = 10 material can be used in future applications to decolorize dyes in textiles industries with previous study of the best experimental conditions like dye concentrations, pH, TiO_2 concentrations, temperature, etc.

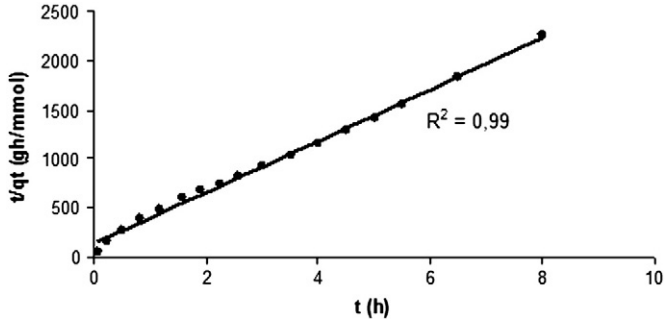

Fig. 10. Effect of TiO_2 dose in the kinetics degradation of MB for TiO_2 R = 10 with 0.4 g of catalyst.

Table 4
Rate constant of pseudo-second order degradation of MB onto R = 10 sample at different initial catalyst content in pH = 10.

Catalyst content (g)	k_{deg} (g/mmol h)	r^2
0.1	126	0.98
0.2	123	0.99
0.3	633	0.99
0.4	495	0.99

Acknowledgements

This work was supported by a grant from the Universidad Nacional del Sur and another from Agencia Nacional de Promoción Científica y Tecnológica de la República Argentina (ANPCyT). CEZ has a grant from the Consejo Nacional de Investigaciones Científicas y Técnicas de la República Argentina (CONICET).

References

[1] N. Koprivanac, A.L. Bozic, S. Papic, Cleaner production processes in the synthesis of blue anthraquinone reactive dyes, Dyes Pigm. 44 (1999) 33–40.
[2] S. Netpradit, P. Thiravetyan, S. Towprayoon, Evaluation of metal hydroxide sludge for reactive dyes adsorption in a fixed-bed column system, Water Res. 38 (2004) 71–78.
[3] M.S. Reisch, Asian textile dye makers are a growing power in changing market, Chem. Eng. News 15 (1996) 10–12.
[4] D.W. Bahnemann, Ultrasmall metal oxide particles: preparation, photophysical characterization, and photocatalytic properties, Isr. J. Chem. 33 (1993) 111–136.
[5] M.R. Hoffmann, S.T. Martin, W. Choi, D.W. Bahnemann, Environmental applications of semiconductor photocatalysis, Chem. Rev. 95 (1995) 69–96.
[6] S. Watson, J. Scott, D. Beydoun, R. Amal, Studies on the preparation of magnetic photocatalysts, J. Nanopart. Res. 7 (2005) 691–705.
[7] Y. Chen, Y. Cao, Y. Bai, W. Yang, J. Yang, H. Jin, T. Li, Study on photoelectric properties of a TiO_2 nanoparticle, J. Vac. Sci. Technol., B 15 (1997) 1442–1444.
[8] S.E. Pratsinis, W. Zhu, S. Vemury, The role of gas mixing in flame synthesis of titania powders, Powder Technol. 86 (1996) 87–93.
[9] V. Rossatto, T. Picatonotto, D. Vione, M.E. Carlotti, Behaviour of some rheological modifiers used in cosmetics under photocatalytic conditions, J. Dispersion Sci. Technol. 24 (2003) 259–271.
[10] J.P. Chen, R.T. Yang, Selective catalytic reduction of NO with NH_3 on SO_4^{2-}/TiO_2 superacid catalyst, J. Catal. 139 (1993) 277–288.
[11] N.N. Rao, S. Dube, Photocatalytic degradation of mixed surfactants and some commercial soap/detergent products using suspended TiO_2 catalyst, J. Mol. Catal. A: Chem. 104 (1996) 197–199.
[12] T. An, J. Liu, G. Li, S. Zhang, H. Zhao, X. Zeng, G. Sheng, J. Fu, Appl. Catal., A 350 (2008) 237–243.
[13] Q. Sheng, S. Yuan, J. Zhang, F. Chen, Microporous Mesoporous Mater. 87 (2006) 177–184.
[14] P.V. Messina, M.A. Morini, M.B. Sierra, P.C. Schulz, Mesoporous silica–titania composed materials, J. Colloid Interface Sci. 300 (2006) 270–278.
[15] P. Van Der Voort, I. Gillis-D'Hamers, E.F. Vansant, Estimation of the distribution of surface hydroxyl groups on silica gel, using chemical modification with trichlorosilane, J. Chem. Soc. Faraday Trans. 86 (1990) 3757–3762.
[16] L. Motte, C. Petit, L. Boulanger, P. Lixon, M.P. Pileni, Synthesis of cadmium sulfide in situ in cadmium bis (2 ethyl hexyl) sulfosuccinate reverse Micelle (1): polydispersity and photochemical reaction, Langmuir 8 (1992) 1049–1053.

[17] M.P. Pileni, L. Motte, C. Petit, Synthesis of cadmium sulfide in situ in reverse micelles: influence of the preparation modes on size, polydispersity, and photochemical reactions, Chem. Mater. 4 (1992) 338–345.
[18] T. Hirai, S. Shiojiri, I. Komasawa, Preparation of metal sulfide composite ultrafine particles in reverse micellar systems and their photocatalytic property, J. Chem. Eng. Jpn. 27 (1994) 590–597.
[19] E.A. El-Sharkwy, A.Y. Soliman, K.M. Al-Amer, Comparative study for the removal of methylene blue via adsorption and photocatalytic degradation, J. Colloid Interface Sci. 310 (2007) 498–508.
[20] Y. Li, G. Demopoulos, Hydrometallurgy 90 (2008) 36-33.
[21] H. Zhuang, J.F. Banfield, Understanding polymorphic phase transformation behaviour during growth of nanocrystalline aggregates: insights from TiO_2, J. Phys. Chem. B (2000) 3481-348.
[22] K.S.W. Sing, D.H. Everett, R.A.W. Haul, L. Moscou, R.A. Pierotti, J. Rouquerol, T. Siemieniewska, Reporting physisorption data for gas/solid systems with special reference to the determination of surface area and porosity, Pure Appl. Chem. 57 (4) (1985) 603–619.
[23] K.S.W. Sing, Reporting physisorption data for gas/solid systems with special reference to the determination of surface area and porosity, Pure Appl. Chem. 57 (1985) 603–619.
[24] M.S. Lee, G.D. Lee, C.S. Ju, S.S. Hong, Preparations of nanosized TiO_2 in reverse microemulsion and their photocatalytic activity, Sol. Energy Mater. Sol. Cells 88 (2005) 389–401.
[25] Y.S. Ho, G. McKay, Sorption of dyes and copper ions onto biosorbents, Process. Biochem. 38 (2003) 1047–1061.
[26] W.J. Weber Jr., J.C. Morris, Kinetics of adsorption on carbon from solution, J. Sanit. Eng. Div. 89 (1963) 31–59.
[27] S. Chin, E. Park, M. Kim, J. Jurng, Photocatalytic degradation of methylene blue with TiO_2 nanoparticles prepared by a thermal decomposition process, Powder Technol. 201 (2010) 171–176.
[28] J. Zhao, H. Hidaka, A. Takamura, E. Pelizzetti, N. Serpone, Photodegradations of surfactants. 1. Zheta-potential measurements in the photocatalytic oxidation of surfactants in aqueous titania dispersions, Langmuir 9 (1993) 1646–1650.
[29] C.C. Chen, C.S. Lu, Y.C. Chung, J.L. Jan, UV light induced photodegradation of malachite green on TiO_2 nanoparticles, J. Hazard. Mater. 141 (2007) 520–528.
[30] B.V. Buxton, C.L. Greenstock, W.P. Helman, A.B. Ross, Critical review of rate constants for reactions of hydrated electrons, hydrogen atoms and hydroxyl radicals in aqueous solution, J. Phys. Chem. 17 (1988) 513–886.
[31] D.C. Hurum, A.G. Agrios, K.A. Gray, T. Rajh, M.C. Thurnauer, Explaining the enhanced photocatalytic activity of degussa P25 mixed-phase TiO_2 using EPR, J. Phys. Chem. B 107 (2003) 4545–4549.
[32] R.I. Bickley, T. Gonzalez Carreño, J.S. Lees, L. Palmisano, R.J. Tilley, A structural investigation of titanium dioxide photocatalysts, J. Solid State Chem. 92 (1991) 178–190.
[33] C.S. Turchi, D.F. Ollis, Photocatalytic degradation of organic water contaminants: mechanisms involving hydroxyl radical attack, J. Catal. 122 (1990) 178–192.
[34] S.S. Hong, C.G. Lim, G.D. Lee, K.T. Lim, B.H. Ahn, A photocatalytic degradation of phenol over TiO_2 prepared by sol–gel method, J. Ind. Eng. Chem. 7 (2001) 99–104.
[35] G.D. Lee, S.K. Jung, Y.J. Jeong, J.H. Park, C.S. Suh, B.H. Ahn, S.S. Hong, Photocatalytic decomposition of 4-nitrophenol over titanium silicalite (TS-1) using hydrogen peroxide as an oxidant, J. Ind. Eng. Chem. 8 (2002) 22–27.
[36] M. Faisal, M. Abu Tariq, M. Muneer, Photocatalysed degradation of two selected dyes in UV-irradiated aqueous suspensions of titania, Dyes Pigm. 72 (2007) 233–239.
[37] C.C. Wong, W. Chu, The direct photolysis and photocatalytic degradation of alachlor at different TiO_2 and UV sources, Chemosphere 50 (2003) 981–987.
[38] J. Liu, T. An, G. Li, N. Bao, G. Sheng, J. Fu, Preparation and characterization of highly active mesoporous TiO_2 photocatalysts by hydrothermal synthesis under weak acid conditions, Microporous Mesoporous Mater. 124 (2009) 197–203.